Journal of Zhejiang University-SCIENCE A (Applied Physics & Engineering)
ISSN 1673-565X (Print); ISSN 1862-1775 (Online)
www.jzus.zju.edu.cn; www.springerlink.com
E-mail: jzus@zju.edu.cn

Experimental investigation of vortex-ring cavitation*

Chen JI, Fang-ye LIN, Jun ZOU†‡

(*State Key Laboratory of Fluid Power and Mechatronic Systems, Zhejiang University, Hangzhou 310027, China*)

†E-mail: junzou@zju.edu.cn

Received July 29, 2016; Revision accepted Oct. 9, 2016; Crosschecked June 12, 2017

Abstract: Vortex-ring cavitation occurs when the pressure inside a torus-shaped core of a vortex ring falls below the vapor pressure of the ambient liquid. By generating a vapor bubble in a rigid tube, a toroidal cavity can be produced outside the tube. The pulsation and propagation behaviors of vortex-ring cavitation are studied using a high-speed video camera and a hydrophone. The experimental results show that the cavity continues to oscillate with a period that depends heavily on the maximal cross-section radius of the cavity and circulation of the vortex flow, under the influence of the surrounding vortex flow field. It is also shown that the cross-radial oscillation of the toroidal cavity can be measured both by a high-speed camera and hydrophone. Moreover, three different methods for estimating the circulation are compared to propose an accurate model of toroidal cavity oscillation. The phenomenon of a toroidal cavity impinging on a fixed wall is also investigated.

Key words: Cavitation; Toroidal cavity; Oscillation period; Impinging on wall
http://dx.doi.org/10.1631/jzus.A1600537 **CLC number:** TH161.12

1 Introduction

Vortex-ring cavitation, induced by a submerged jet, is a less common phenomenon that makes the jet more erosive than a single-phase liquid jet. The pressure oscillations of cavitation bubbles can enhance erosion effects due to the frequently varying pressure field, which is very effective in various applications such as rock cutting, underwater cleaning (Genoux and Chahine, 1984; Johnson *et al*., 1984a; 1984b), and underwater sound generation (Chahine *et al*., 1985). In certain cases, the pressure pulsation produces a toroidal cavity around the nozzle, instead of the ring-shaped cavitation cloud. The toroidal cavity occurs when the pressure inside the core of vortex ring drops below the vapor pressure of the ambient liquid, showing a clear gas-liquid interface. Although the physics of a spherical cavitation bubble could be well established by numerical models (Lauterborn and Kurz, 2010; Wang, 2014; Jiang *et al*., 2015), very few studies have been conducted on the behaviors of ring-shaped cavities. Teslenko *et al.* (2014) reported that the emergence of a toroidal cavity is significantly dependent on the velocity of the jet. Chahine and Genoux (1983a) proposed a theoretical model of the toroidal cavity that provides a method to predict the oscillation period and amplitude of its cross section. However, the accuracy of the theoretical model is limited by the estimation of important factors such as circulation, and there are few quantitative experiments focusing on the radial oscillation of the toroidal cavities.

This study aims to present a detailed experimental description of the behaviors of toroidal cavities produced by a cavitation bubble in a rigid tube. By comparing the theoretical model and experimental results, the effect of radial oscillation is

‡ Corresponding author

* Project supported by the National Natural Science Foundation of China (Nos. 51475415 and 51405429), the Zhejiang Provincial Natural Science Foundation for Distinguished Young Scholars (No. LR15E050001), and the Science Fund for Creative Research Groups of the National Natural Science Foundation of China (No. 51521064)

ORCID: Jun ZOU, http://orcid.org/0000-0003-2443-3516

addressed. A simple revision of the circulation model is proposed, leading to a better prediction of the oscillation period. In addition, the phenomenon of a toroidal cavity impinging on a wall is investigated.

2 Experimental setup

A schematic diagram of the experimental setup is shown in Fig. 1. A circuit is used to induce a low-voltage electric spark in a transparent cylindrical tube immersed in tap water (Xu *et al*., 2014; Hu *et al*., 2016a; 2016b), to generate a cavitation bubble in the tube. One open end of the tube is blocked by a silica gel plug pierced by electrodes, which encourages the formation of a toroidal cavity around the other open end. The behavior of the cavity is recorded by a high-speed camera (FASTCAM-ultima APX, San Diego, USA) fitted with a Nikkor 60-mm microlens, at a speed of 24000 or 8000 frames per second for a large frame. Our experimental data are thus divided into two parts: high-speed image data with a resolution of 0.077 mm/pixel for free oscillation experiments and low-speed but large-frame image data with a resolution of 0.101 mm/pixel for wall impingement experiments. Backlight is produced by a high-intensity light-emitting diode (LED) lamp covered by a diffuser (Hu *et al*., 2016a; 2016b). All the experiments are conducted at atmospheric pressure, and the laboratory temperature is maintained at (25±2) °C. The density of the liquid ρ is 997 kg/m^3, and the surface tension σ is 0.073 N·m. Three types of tubes are employed in the experiments, with inside diameters D_t of 4.12, 5.20, and 6.20 mm and outside diameters of 6.15, 7.90, and 8.90 mm, respectively, and the length of all tubes is 45 mm. The distance from the spark generation point to the end of the tube varies from 15 mm to 25 mm.

For the wall impingement experiments, the tube is placed perpendicular to an acrylic wall at a distance of 100–150 mm. In addition, a hydrophone with a resolution of 100000 Hz is used to obtain a comprehensive understanding of the toroidal cavity from its generation to its dissipation near the wall. Sound-absorbing foam is pasted on the wall of the tank (not including the photo-recording region) to reduce the disturbance caused by reflection.

The cavity in the experiments is affected by Rayleigh instability, leading to a slight distortion of the cavitating ring, as shown in Fig. 2a. In this study, the cavitation volume is simplified as an axis-symmetrical toroidal cavity whose cross section shape is assumed to be circular. The average radius of its cross section R can be evaluated as

$$R(t)=\frac{1}{2}H(t),$$

where $H(t)$ is the average thickness of the toroidal cavity measured from photos, as shown in Fig. 2. The overall radius of the cavity centerline, $A(t)$, is estimated as

$$A(t)=\frac{1}{2}(D(t)-H(t)),$$

where $D(t)$ is the external diameter of the toroidal cavity. In particular, A_0, R_0, H_0, and D_0 represent the maximum values of $A(t)$, $R(t)$, $H(t)$, and $D(t)$, respectively. A shape coefficient ε is defined to describe the ratio between the cross radius and overall radius of the toroidal cavity, as $\varepsilon=R_0/A_0$. The axial distance between the toroidal cavity and the nearest tube ending is noted as $S(t)$.

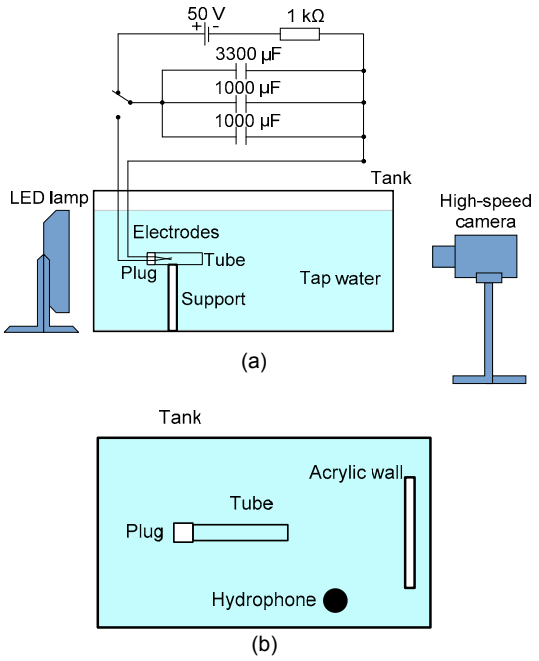

Fig. 1 Schematic diagram of the experimental setup
(a) Experimental setup for free oscillation experiments; (b) Hydrophone and acrylic wall in the wall impinging experiments

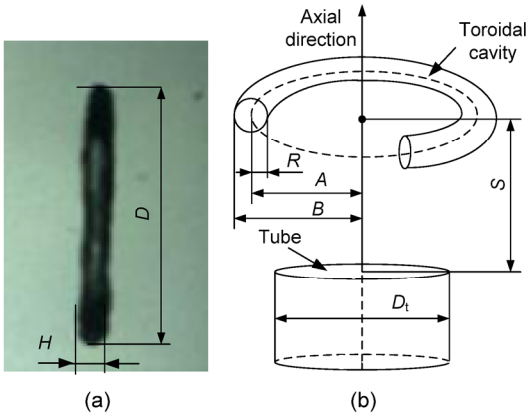

Fig. 2 Schematic of toroidal cavity
(a) Side view of a cavity captured by high-speed camera; (b) Schematic of a toroidal cavity generated outside the end of the tube

3 Results and discussion

For the free oscillating toroidal cavity experiments, the typical development of a toroidal vapor cavity is shown in Fig. 3, where the moment of the electric spark is set as time t=0. A toroidal vapor cavity forms near the end of the tube, while the cavitation bubble inside the tube (termed the inner bubble in this study) expands. Once generated, the toroidal cavity continues moving away from the tube ending in the axial direction. When it first appears, the overall radius A is close to the internal radius of the tube, and the toroidal cavity then expands in both the overall and cross radial directions. After the inner bubble reaches its largest volume at 1.042 ms, the toroidal cavity begins to shrink. Throughout the oscillation period of the inner bubble, i.e., from 0 to 2.542 ms in Fig. 3, the toroidal cavity undergoes three cycles of expansion-contraction. At t=2.542 ms, the collapse of the inner bubble produces a shockwave, causing an obvious compression of the cavity. The rebound of the inner bubble is quite weak, with negligible effect on the oscillation of the toroidal cavity, which continues moving axially and oscillating radially.

Fig. 4a shows the first five oscillation periods of the toroidal cavity in Fig. 3. The distance between the end of the tube and the cavity, $S(t)$, is nearly a regular ramp function, which implies that the toroidal cavity translates with an approximately constant speed V_z, on which the expansion and collapse of the inner bubble has no effect. At t=2.542 ms, which is t_c in Fig. 4a, the inner bubble collapses to its minimum volume. A dimensionless thickness, $\chi = 2(H(t) - \bar{H})/\Delta H$, is used to measure the cross radial oscillation in a unit form, as shown in Fig. 4b, which depicts the mean thickness and oscillation amplitude in the first period after t_c. The time t_c divides the oscillation process of the toroidal cavity into two stages. During the early stage, the oscillation is significantly affected by the inner bubble, leading to several irregular oscillating periods. After t_c, however, the energy dissipation significantly weakens the influence of the inner bubble on the toroidal cavity, and both the frequency and the amplitude of the average thickness H become fairly stable, especially for a weak toroidal cavity (dashed line in Fig. 4b). The minimum value of H in this stable stage appears at t_c, due to the shockwave produced by the collapse of the inner bubble. The external radius $B(t)$, the thickness $H(t)$, and the overall radius $A(t)$ show a similar oscillation period during the stable stage, but the oscillation phases of $H(t)$ and $A(t)$ are nearly reversed.

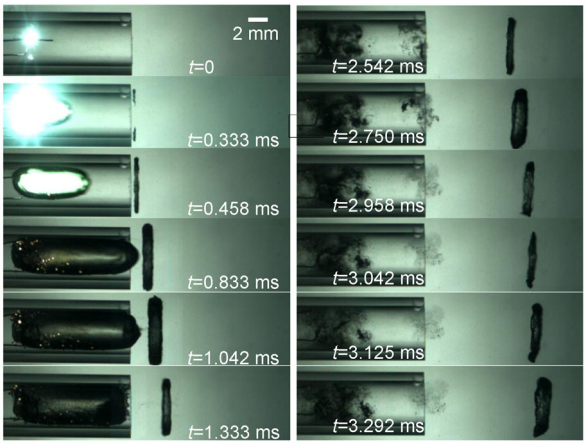

Fig. 3 Sequence of the oscillating toroidal cavity
The largest length of the inner cavitation bubble is 16.5 mm, while the distance from the spark point to the end of the tube is 13.2 mm. The tube used here has an inside diameter D_t of 5.20 mm, and the reference circulation Γ_{ref} in this case is 0.0522 m^2/s

The oscillation of a ring-shaped cavity was modeled by Chahine and Genoux (1983b), using the method of matched asymptotic expansions. It was claimed that the dynamics of the cavity follows an equation analogous to the Rayleigh-Plesset equation:

$$(R\ddot{R}+\dot{R}^2)\ln\frac{R}{8A_0}+\frac{1}{2}\dot{R}^2 =\frac{1}{\rho}\left[P_0-\frac{\rho}{2}\left(\frac{\Gamma}{2\pi R}\right)^2-P_v-P_{g0}\left(\frac{R_0}{R}\right)^{2k}+\frac{\sigma}{R}\right], \quad (1)$$

where k stands for the polytropic exponent that characterizes the thermodynamic evolution of gas; Γ is the circulation; P_{g0} is the partial pressure of non-condensable gas, 980.8 Pa; P_0 is the environmental pressure, maintained at 101 kPa; P_v is the vapor pressure of water, 1.96×10^3 Pa. Eq. (1) focuses on the pulsation of R, while the oscillation of A is assumed to be negligible. In this study, however, the oscillation amplitude of the overall radius ΔA has the same order of magnitude as ΔH, as shown in Fig. 4. The experimental results related to the variation of A are shown in Fig. 5, where the shape ratio ε ranges from 0.05 to 0.35. The average overall radius $\overline{A}$ (during the stable stage) depends solely on the tube diameter. A simple correlation of $\overline{A}\sim0.54D_t$ agrees well with the results for every tube diameter employed. On the other hand, the relative oscillation amplitude of $\Delta A/\overline{A}$ varies linearly with ε, as shown in Fig. 5b. By fitting the experimental data, the oscillation of A can be evaluated as $\Delta A/\overline{A}=0.51\varepsilon$.

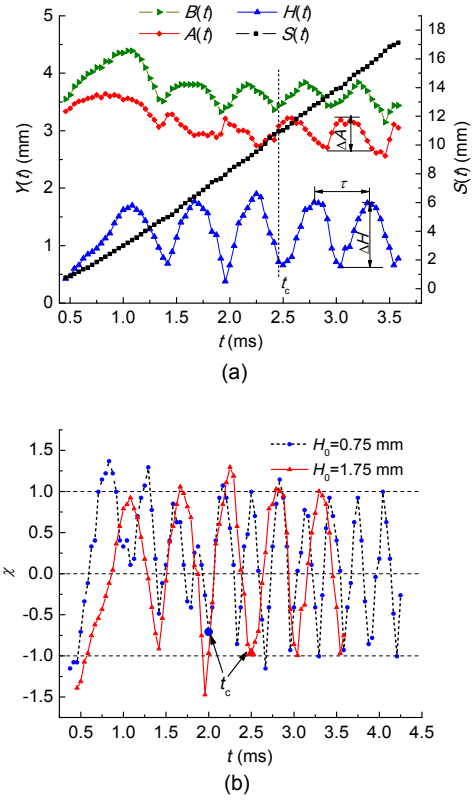

Fig. 4 (a) Temporal variation of toroidal cavity parameters corresponding to Fig. 3 (the left vertical axis $Y(t)$ represents $B(t)$, $A(t)$, and $H(t)$; V_z=5.43 m/s, H_0=1.75 mm, τ=0.5 ms); (b) Two cases of the dimensionless thickness of the toroidal cavity in relation to time (the solid line represents the case in Fig. 4a, and the dashed line represents a toroidal cavity with V_z=4.03 m/s, H_0=0.75 mm, and τ=0.25 ms; the large symbols correspond to t_c)

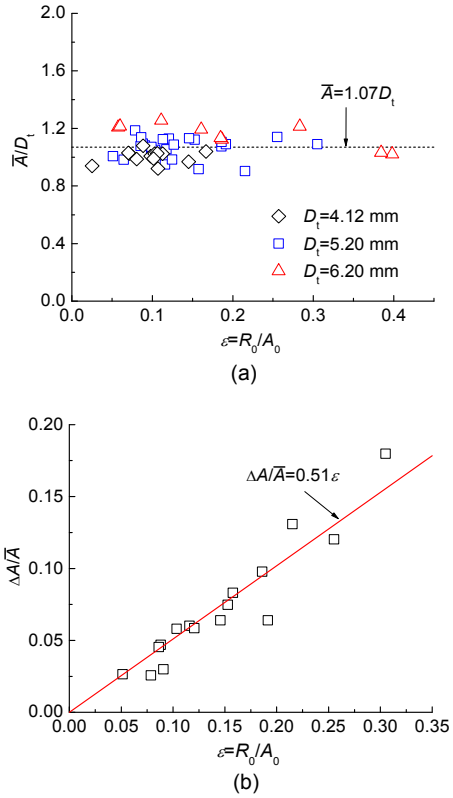

Fig. 5 Characteristics of ring vortex cavity with macroscopic radius: (a) ratio between average overall radius $\overline{A}$ and diameter; (b) oscillation amplitude of A against ε

According to Chahine and Genoux (1983b), the assumption of a constant A in Eq. (1) leads to a scale law of $\tau\sim M$, where M is a characteristic time depending on the geometry of the toroidal cavity, as $M=R_0(\rho/\Delta P)^{0.5}[\ln(8/\varepsilon)]^{0.5}$, where $\Delta P=P_0-P_v$. The scale law can be used to describe the pulsation period of the cavity, so it is of interest to test its accuracy in cases with relatively strong oscillation of the overall radius. As shown in Fig. 6, the linear correlation still agrees well with the experimental results, while the error

becomes larger with increasing M. This conclusion implies that the interaction between radial oscillation and cross oscillation is rather weak, and therefore Eq. (1) can be used to model the oscillation of the cross section radius R.

To apply Eq. (1) to the dynamic analysis of the toroidal cavity, the circulation Γ around the cross section of the cavity must be evaluated. Two methods have been established in the literature for evaluating the parameter Γ. The first method is based on a simple line vortex model, assuming that the surrounding flow field of the cavity is analogous to a vortex ring with a line core (Shariff and Leonard, 1992; Dziedzic and Leutheusser, 1996). According to the Biot-Savart law, the circulation is

$$\Gamma_1=2R_0V_z, \tag{2}$$

where V_z is the translation velocity of the toroidal cavity.

The second method is proposed by Chahine and Genoux (1983b), based on the following equation:

$$\left(\varepsilon\log\frac{8}{\varepsilon}-\frac{1}{2}\varepsilon\right)\Gamma_2^2-4\pi R_0V_z\Gamma_2+\frac{4\pi R_0\sigma}{\rho}=0. \tag{3}$$

In cases at millimeter scale, the effect of surface tension is negligible, and therefore Eq. (3) is the same as the hollow core model of the vortex ring (Sullivan *et al*., 2008). The circulation is

$$\Gamma_2=\frac{4\pi R_0V_z}{\left(\varepsilon\log\frac{8}{\varepsilon}-\frac{1}{2}\varepsilon\right)}. \tag{4}$$

The equations for Γ_1 and Γ_2 are applied to the corresponding experimental cases. In addition, a reference circulation Γ_{ref} is calculated from the experimental results of τ by the method of Newton iteration. Fig. 7a compares the calculated circulation and the reference value. Eq. (2) usually underestimates the circulation, while the results of Eq. (4) are always larger than Γ_{ref}. Fig. 7b shows the numerical solution of a typical case of ε=0.305, where Γ_1 and Γ_2 are used in Eq. (1). The deviation between Γ_{ref} and the evaluated circulations leads to wrong results for both the amplitude and the frequency of the oscillation, proving that an appropriate estimation method for Γ is important. The calculation of Γ_2 accounts for the void vortex core, based on the assumption that the sizes of both the entire cavity and the void core are negligible. In the case of a toroidal cavity, the vortex core is an oscillating toroidal cavitation bubble, and therefore the circulation will be overestimated using the values of R_0 and ε. Based on the experimental results in this study, the accuracy of the circulation can be improved by replacing the average factors of R_0 and ε in Eq. (4) with the minimal values during the oscillation of the toroidal cavity. The revised equation is

$$\Gamma_3=\frac{4\pi R_1V_z}{\left(\varepsilon_1\log\frac{8}{\varepsilon_1}-\frac{1}{2}\varepsilon_1\right)}, \tag{5}$$

where $\varepsilon_1=R_1/A_1$, and R_1 and A_1 are the cross-section radius and overall radius of the toroidal cavity at its minimal size, respectively. The results of Γ_3 are always between Γ_1 and Γ_2 and agree better with the experiments, as shown in Fig. 7. Therefore, Eqs. (1) and (5) constitute an estimation model for the oscillation of the toroidal cavity.

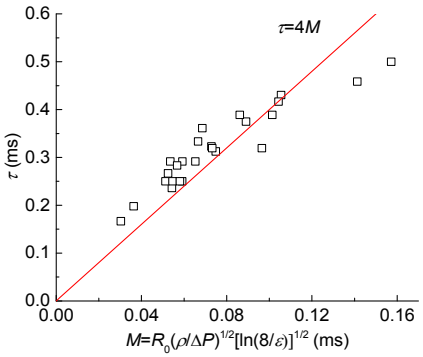

Fig. 6 Oscillation period τ against characteristic time M

With the basic understanding of vortex-ring cavitation mentioned above, we investigate the phenomenon of a toroidal cavity impinging on a fixed wall. The toroidal cavities investigated varied in the following ranges: ε: 0.03–0.3, R_0: 0.1–0.75 mm, and V_z: 3–5 m/s. Similarly to a non-cavitating vortex ring impinging on a wall (Walker *et al.*, 1987; Xu *et al.*, 2013), as a toroidal cavity approaches a wall, the center of the cavity (or vortex ring) slows down and finally oscillates weakly near the wall at a distance of 1.2 mm (Fig. 8). The toroidal cavities maintain a

limited distance of 1.0–1.5 mm from the wall in all our experiments. Moreover, the cavity is stretched along the overall radial direction, which means that the overall radius $A(t)$ increases under the influence of a wall. The cavity shrinks and breaks up into a number of discrete cavities. Eventually, it disappears due to energy dissipation, while $A(t)$ reaches its maximum value A_{max}.

The maximum expansion ratio of the cavity impinging on a wall, $\alpha=A_{max}/A_0$, varying with ε, is shown in Fig. 9. Our experimental results fit well, with a scaling law of $\alpha\sim\varepsilon^{0.25}$.

With the help of a hydrophone, a comprehensive investigation of the toroidal cavity oscillation is viable. The time history of the toroidal cavity from its generation to its dissipation near the wall is shown in Fig. 10a. The low-frequency noise (below 200 Hz) is eliminated by a high-pass filter. The inner bubble expands to its largest volume at t_1 and collapses at t_c. The overall radius of the toroidal cavity increases when the vortex ring is significantly affected by the wall at t_2. Regular oscillation periods are observed between t_c and t_2, while the amplitude decreases when the cavity moves away from the hydrophone. Moreover, the fast Fourier transform (FFT) is used to reveal the spectral characteristics during the regular oscillation periods (t_c–t_2). The oscillation frequency measured by hydrophone is 2150 Hz (Fig. 10c), which is approximately the same as the value measured by image, 2222 Hz. Thus, the cross radial oscillation can be measured both by high-speed camera and by hydrophone. As the cavity approaches the wall, intense fluctuation appears (Fig. 10b), and the oscillation becomes non-periodic.

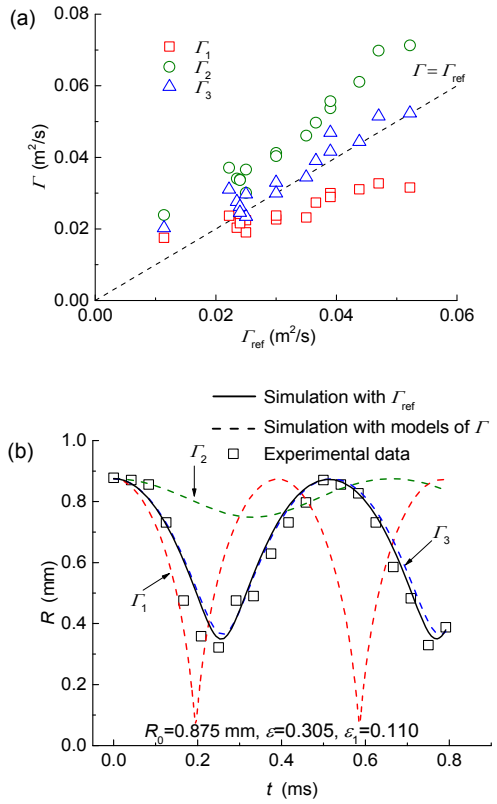

Fig. 7 Circulation for vortex ring estimated by three methods: (a) comparison of the three models with Γ_{ref}; (b) a typical case of ε=0.305, D_t=5.20 mm

The experimental results are shown as squares, while the simulation curves from three different circulation models are shown as dashed lines

4 Conclusions

The oscillation of toroidal cavities induced by vortex rings is investigated experimentally. An

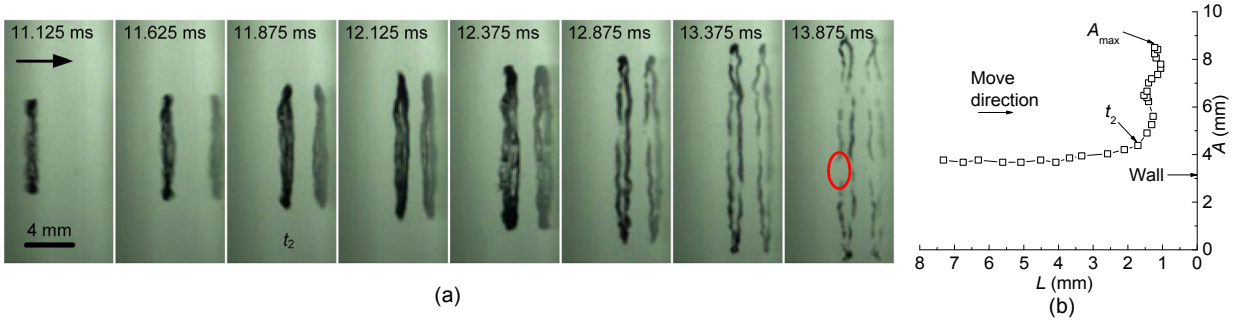

Fig. 8 A toroidal cavity impinging on a fixed wall (from left to right)

(a) Mirror images seen on the right side of the cavity due to the reflection effect of the wall (the cavity occupied here has a size H_0=1.4 mm, A_0=3.57 mm, a translation velocity V_z=4.86 m/s, and an oscillation frequency f=2200 Hz before impact; the circle denotes that the toroidal cavity collapses and breaks up into a number of discrete cavities); (b) Trajectory of the cavity in Fig. 8a (L is the distance from the center of the toroidal cavity to the wall; points are 0.125 ms apart)

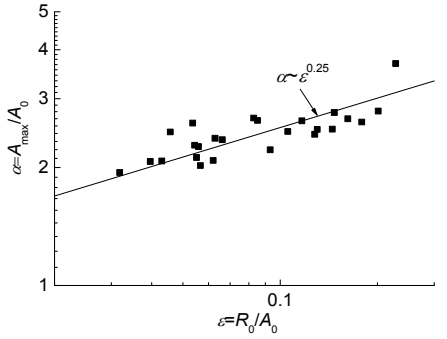

Fig. 9 The maximum expansion ratio of the cavity impinging on a wall, $\alpha=A_{max}/A_0$, varying with ε

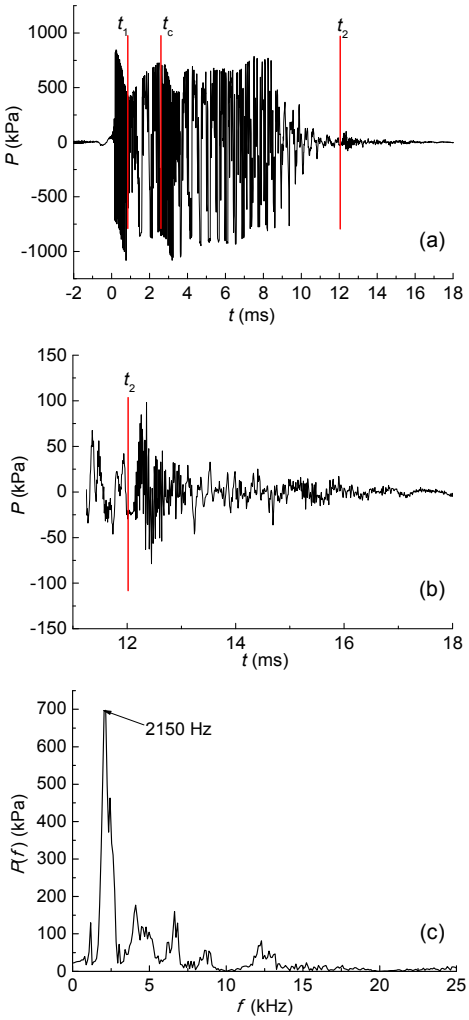

Fig. 10 Time history and spectrum of the oscillating cavity in Fig. 8: (a) time history of the toroidal cavity from its generation to its dissipation near the wall (the inner bubble expands to its largest volume at t_1 and collapses at t_c; the ring radius of the toroidal cavity increases when the vortex ring is affected by the wall at t_2); (b) partial enlargement of Fig. 8a; (c) spectrum recorded by hydrophone in the region t_c–t_2

approximate constant translation speed and a steady oscillation period are observed in the experiments, and the cross radial oscillation of the toroidal cavity can be measured both by high-speed camera and by hydrophone. The overall radius of the toroidal cavity oscillates with an amplitude of $\Delta A/\bar{A}\sim\varepsilon$, which can be neglected when $\varepsilon\ll1$. The experimental data agree well with the theoretical analysis: $\tau\sim R_0(\rho/\Delta P)^{0.5}\times[\ln(8/\varepsilon)]^{0.5}$. By comparing three equations and the experimental results, an estimation model of circulation is proposed, which is calculated as Eq. (5). Furthermore, when a toroidal cavity impinges on a fixed wall, the experimental results show that the maximum expansion ratio of the cross radius has a scaling law of $\alpha\sim\varepsilon^{0.25}$.

References

Chahine, G.L., Genoux, P.F., 1983a. Collapse of a cavitating vortex ring. *Journal of Fluids Engineering*, **105**(4):400-405. http://dx.doi.org/10.1115/1.3241018

Chahine, G.L., Genoux, P.F., 1983b. Static and dynamic quilibrium of a vaporous vortex-ring. *Journal de Mecanique Theorique et Appliquee*, **2**(5):829-857 (in French).

Chahine, G.L., Johnson, V.E., Lindenmuth, W.T., *et al*., 1985. The use of self-resonating cavitating water jets for underwater sound generation. *The Journal of the Acoustical Society of America*, **77**(1):113-126. http://dx.doi.org/10.1121/1.392274

Dziedzic, M., Leutheusser, H.J., 1996. An experimental study of viscous vortex rings. *Experiments in Fluids*, **21**(5): 315-324. http://dx.doi.org/10.1007/BF00189051

Genoux, P.F., Chahine, G.L., 1984. Collapse of a toroidal bubble near a solid wall. ASME Cavitation and Multiphase Flow Forum, p.69-72.

Hu, L., Shen, Y.N., Chen, W.Y., *et al*., 2016a. Experimental investigation on submerged gas-liquid mixture injection into water through a micro-channel. *International Journal of Multiphase Flow*, **83**:39-50. http://dx.doi.org/10.1016/j.ijmultiphaseflow.2016.03.012

Hu, L., Liu, Q., Chen, W.Y., *et al*., 2016b. Normalizing study on the characteristic size of the stable cavity induced by a gas-jet penetrating into a liquid sheet. *Experimental Thermal and Fluid Science*, **70**:228-235. http://dx.doi.org/10.1016/j.expthermflusci.2015.09.017

Jiang, L., Ge, H., Feng, C.L., *et al*., 2015. Numerical simulation of underwater explosion bubble with a refined interface treatment. *Science China Physics, Mechanics & Astronomy*, **58**(4):1-10. http://dx.doi.org/10.1007/s11433-014-5616-9

Johnson, V.E.Jr., Chahine, G.L., Lindenmuth, W.T., *et al*.,

1984a. Cavitating and structured jets for mechanical bits to increase drilling rate—part I: theory and concepts. *Journal of Energy Resources Technology*, **106**(2):282-288. http://dx.doi.org/10.1115/1.3231053

Johnson, V.E.Jr., Chahine, G.L., Lindenmuth, W.T., *et al*., 1984b. Cavitating and structured jets for mechanical bits to increase drilling rate—part II: experimental results. *Journal of Energy Resources Technology*, **106**(2):289-294. http://dx.doi.org/10.1115/1.3231054

Lauterborn, W., Kurz, T., 2010. Physics of bubble oscillations. *Reports on Progress in Physics*, **73**(10):106501. http://dx.doi.org/10.1088/0034-4885/73/10/106501

Shariff, K., Leonard, A., 1992. Vortex rings. *Annual Review of Fluid Mechanics*, **24**(1):235-279. http://dx.doi.org/10.1146/annurev.fl.24.010192.001315

Sullivan, I.S., Niemela, J.J., Hershberger, R.E., *et al*., 2008. Dynamics of thin vortex rings. *Journal of Fluid Mechanics*, **609**:319-347. http://dx.doi.org/10.1017/S0022112008002292

Teslenko, V.S., Drozhzhin, A.P., Medvedev, R.N., 2014. Pulsation of cavitating vortex rings in water. *Technical Physics Letters*, **40**(11):1021-1023. http://dx.doi.org/10.1134/S1063785014110297

Walker, J.D.A., Smith, C.R., Doligalski, T.L., *et al*., 1987. The impact of a vortex ring on a wall. *Journal of Fluid Mechanics*, **181**:99-140. http://dx.doi.org/10.1017/S0022112087002027

Wang, Q.X., 2014. Multi-oscillations of a bubble in a compressible liquid near a rigid boundary. *Journal of Fluid Mechanics*, **745**:509-536. http://dx.doi.org/10.1017/jfm.2014.105

Xu, M., Ji, C., Zou, J., *et al*., 2014. Particle removal by a single cavitation bubble. *Science China Physics, Mechanics and Astronomy*, **57**(4):668-673. http://dx.doi.org/10.1007/s11433-013-5192-4

Xu, Y., Feng, L.H., Wang, J.J., 2013. Experimental investigation of a synthetic jet impinging on a fixed wall. *Experiments in Fluids*, **54**:1512. http://dx.doi.org/10.1007/s00348-013-1512-8

中文概要

题　目： 涡环空化的实验研究

目　的： 研究涡环空化产生的环状空泡的振荡周期及其冲击壁面溃灭的动态过程。

创新点： 1. 通过实验方法，比较几种不同的速度环量计算模型在环状空泡振荡控制方程中的适用性。2. 通过声学方法，得到环状空泡在撞击壁面溃灭过程中的频谱特征。

方　法： 1. 通过管内空泡膨胀产生高速射流；高速射流在管口处形成涡环并发生涡环空化。2. 基于高速摄像进行流体分析。

结　论： 1. 在管内空泡溃灭后，环状空泡以恒定速度沿管的轴向运动，且其振荡周期几乎保持不变。2. 环状空泡的振荡周期基本上满足规律：$\tau\sim R_0(\rho/\Delta P)^{0.5}[\ln(8/\varepsilon)]^{0.5}$。3. 在空泡振荡的最小直径为特征直径；根据空心涡核模型，可以计算得到最接近实验结果的速度环量值。4. 当空泡冲击壁面时，空泡的环向直径将变大。5. 环向直径的最大扩张比α与其截面直径与环向直径的比ε相关：$\alpha\sim\varepsilon^{0.25}$。

关键词： 空化；环状空泡；振荡周期；壁面冲击